# Bent by baryons: the low mass galaxy-halo relation

Till Sawala[1]*, Carlos S. Frenk[1], Azadeh Fattahi[2], Julio F. Navarro[2], Richard G. Bower[1], Robert A. Crain[3], Claudio Dalla Vecchia[4], Michelle Furlong[1], Adrian Jenkins[1], Ian G. McCarthy[5], Yan Qu[1], Matthieu Schaller[1], Joop Schaye[3] and Tom Theuns [1,6]

[1] *Institute for Computational Cosmology, Department of Physics, University of Durham, South Road, Durham DH13LE, UK*
[2] *Department of Physics and Astronomy, University of Victoria, 3800 Finnerty Road, Victoria, British Columbia V8P 5C2, Canada*
[3] *Leiden Observatory, Leiden University, Postbus 9513, 2300 RA Leiden, The Netherlands*
[4] *Instituto de Astrofísica de Canarias, C/ Vía Láctea s/n, 38205 La Laguna, Tenerife, Spain*
[5] *Astrophysics Research Institute, Liverpool John Moores University, 146 Brownlow Hill, Liverpool L3 5RF*
[6] *Department of Physics, University of Antwerp, Campus Groenenborger, Groenenborgerlaan 171, B-2020 Antwerp, Belgium*

**ABSTRACT**

The relation between galaxies and dark matter halos is of vital importance for evaluating theoretical predictions of structure formation and galaxy formation physics. We show that the widely used method of abundance matching based on dark matter only simulations fails at the low mass end because two of its underlying assumptions are broken: only a small fraction of low mass ($< 10^{9.5} \mathrm{M}_\odot$) halos host a visible galaxy, and halos grow at a lower rate due to the effect of baryons. In this regime, reliance on dark matter only simulations for abundance matching is neither accurate nor self-consistent. We find that the reported discrepancy between observational estimates of the halo masses of dwarf galaxies and the values predicted by abundance matching does not point to a failure of ΛCDM, but simply to a failure to account for baryonic effects. Our results also imply that the Local Group contains only a few hundred observable galaxies in contrast with the thousands of faint dwarfs that abundance matching would suggest. We show how relations derived from abundance matching can be corrected, so that they can be used self-consistently to calibrate models of galaxy formation.

**Key words:** cosmology: theory – galaxies: formation – galaxies: evolution – galaxies: mass functions – methods: N-body simulations

## 1 INTRODUCTION

In the ΛCDM paradigm (e.g. Davis et al. 1985; Frenk et al. 1988), stars form as gas cools in collapsed dark matter halos (e.g. White & Rees 1978; White & Frenk 1991). The formation of galaxies involves both baryons and dark matter, but while only gas and stars are directly observable, numerical simulations of structure formation have largely been limited to the dark matter component, under the assumption that gravity is the only relevant force on large scales.

A conceptually simple and yet very powerful method to connect galaxies and halos in this scenario, which does not require any detailed knowledge of the complex physics of galaxy formation, is abundance matching (e.g. Frenk et al. 1988; Yang et al. 2003; Kravtsov et al. 2004; Vale & Ostriker 2006; Moster et al. 2010; Guo et al. 2010; Behroozi

et al. 2013; Moster et al. 2013). Assuming that a monotonic relation exists between some observable property of a galaxy (such as stellar mass) and some property of its dark matter halo (such as total mass), the relationship between both quantities can be computed from:

$$\int_{\mathrm{a_{h,min}}}^{\mathrm{a_{h,max}}} N_h(a_h) da_h = \int_{\mathrm{a_{\star,min}}}^{\mathrm{a_{\star,max}}} N_\star(a_\star) da_\star, \qquad (1)$$

where $N_h(a_h)$ and $N_\star(a_\star)$ are the numbers of halos and galaxies in the same volume, with properties $a_h$ and $a_\star$, whose maxima determine the upper limits $\mathrm{a_{h,max}}$ and $\mathrm{a_{\star,max}}$. For any lower limit, $\mathrm{a_{h,min}}$, a corresponding lower limit, $\mathrm{a_{\star,min}}$, is chosen such that Eq. 1 is satisfied, and the average relation $a_\star(a_h)$ is then uniquely determined.

Abundance matching is employed widely to infer quantities such as the stellar-to-total mass relation (e.g. Frenk et al. 1988; Yang et al. 2003; Guo et al. 2010; Moster et al. 2013). It has also been used to constrain the mass of the
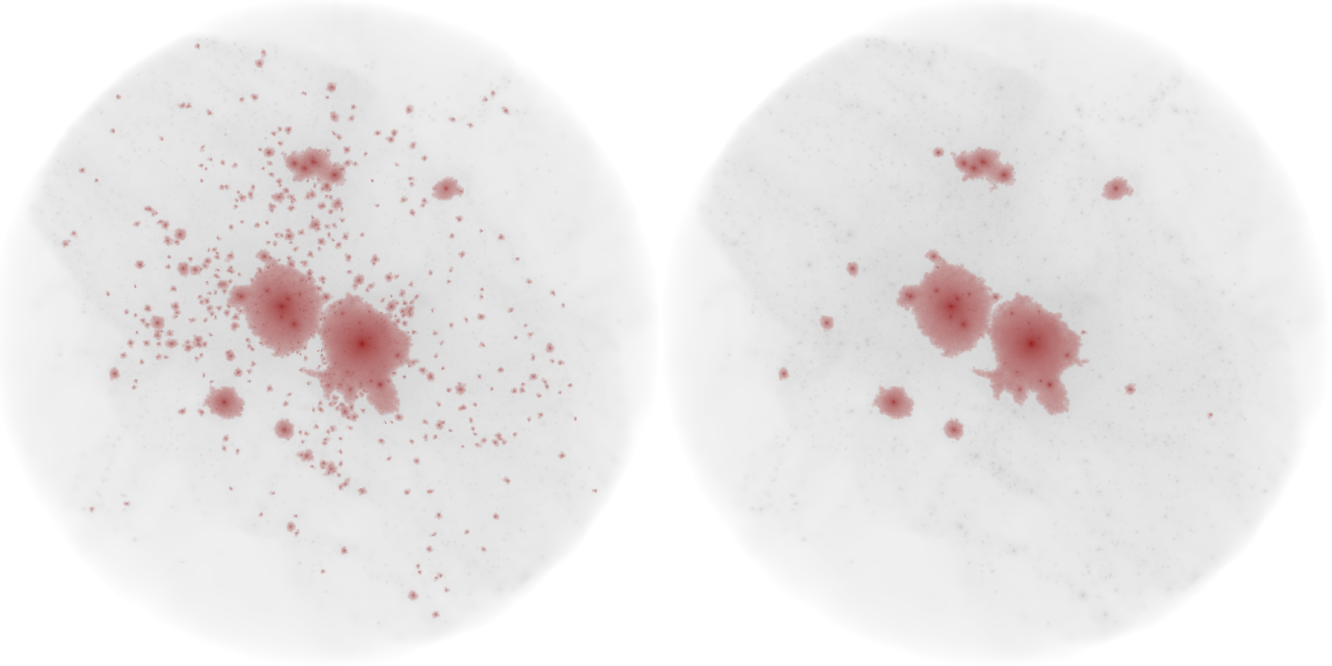
* E-mail: `till.sawala@durham.ac.uk`

**Figure 1.** Projected density distribution of dark matter within 2 Mpc around the simulated Milky Way - M31 barycentre at $z = 0$ from one of our simulation volumes. Highlighted in red on top of the total mass distribution are particles in halos above $5 \times 10^7 \mathrm{M_\odot}$ (left panel), and particles in just those halos that contain stars (right panel).

Milky Way's halo from its stellar mass (Guo et al. 2010), and to predict the total number of dwarf galaxies in the Local Group from an N-body simulation (Garrison-Kimmel et al. 2014).

Generally regarded as assumption-free, abundance matching results are often interpreted as direct predictions of the underlying cosmological model. They have also been used as a benchmark for models of galaxy formation physics, such as semi-analytic models (e.g. Guo et al. 2011), and to calibrate hydrodynamic simulations (e.g. Scannapieco et al. 2012; Munshi et al. 2013). However, models that reproduce the abundance matching relation for low-mass galaxies often require very strong feedback, which can result in an unrealistically high passive fraction (Fontanot et al. 2009; Weinmann et al. 2012; Moster et al. 2013). Conversely, many hydrodynamical simulations that produce realistic dwarf galaxies appear to have halo masses significantly below those inferred by abundance matching (e.g. Sawala et al. 2011; Avila-Reese et al. 2011).

In some cases, the stellar-to-total mass relation derived from abundance matching can also be compared directly to observations of individual galaxies. While they agree for galaxies in halos more massive than $\sim 10^{12} \mathrm{M_\odot}$ (Guo et al. 2010), discrepancies have been reported for lower mass halos (Ferrero et al. 2012). In particular, dynamical mass estimates derived from stellar kinematics suggest stellar-to-total mass ratios for individual dwarf galaxies which are an order of magnitude higher than those inferred from abundance matching in ΛCDM.

Recently, we have shown that simulations that model the evolution of dark matter and baryons as a single fluid subject only to gravity (henceforth referred to as "Dark Matter Only" or DMO simulations) do not produce the same abundance of halos as hydrodynamic simulations that include the full baryonic effects. In particular, the collapse and subsequent expulsion of baryons by feedback processes reduce the mass of individual halos (Sawala et al. 2013), a result that has since been reproduced and extended to higher masses (Velliscig et al. 2014; Cui et al. 2014).

Here we use a new set of high-resolution hydrodynamical simulations of Local Group volumes to explore how the results of abundance matching are affected when the effects of baryons and the appearance of dark halos are included self-consistently. Unlike models that are calibrated to reproduce an abundance matching relation based on a DMO simulation *before* baryons are taken into account, the stellar-to-total mass relation produced in our simulations is consistent with the relation we derive from abundance matching *after* the effects of baryons are included. Furthermore, this relation agrees with the dwarf galaxy data, thus demonstrating that the reported high stellar-to-total mass ratios of these galaxies are entirely consistent with the ΛCDM model.

This paper is organised as follows. In Section 2, we describe the simulations on which our work is based. In Section 3, we describe our results: the fraction of halos that host galaxies is discussed in Section 3.1, the application to abundance matching in Section 3.2, and the implications in Section 3.3. We conclude with a summary in Section 4.

## 2    METHODS

We use a suite of cosmological "zoom" simulations that each contain a pair of galaxies in halos of $\sim 10^{12} \mathrm{M_\odot}$ in a Local Group environment (see Fig. 1). In particular, we require that each volume contain two halos of $5 \times 10^{11} - 2.5 \times 10^{12} \mathrm{M_\odot}$ separated by $800 \pm 200$ kpc, approaching with radial veloc-

ity of $0 - 250$ kms$^{-1}$ and with tangential velocity below 100 kms$^{-1}$ in an environment with an unperturbed Hubble flow out to 4 Mpc. A total of 12 volumes were selected from the DOVE simulation, a $100^3$Mpc$^3$ N-Body simulation based on the WMAP-7 cosmology. The cosmological parameters and the linear phases of DOVE, which are taken from the public multi-scale Gaussian white noise field PANPHASIA, are given in tables 1 and 6 of Jenkins (2013), which also describes the method used to make the Local Group zoom initial conditions. The high resolution initial conditions were set up using second-order Lagrangian perturbation theory as described in Jenkins (2010).

The simulations were performed using a pressure-entropy variant (Hopkins 2013) of the Tree-PM SPH code P-GADGET3 (Springel 2005), described in Dalla Vecchia et al. 2014 (in prep.). The subgrid physics model is an improved version of the model used in the *OverWhelmingly Large Simulations* project (OWLS; Schaye et al. 2010), that has been developed for the *Evolution and Assembly of GaLaxies and their Environments project* (EAGLE, Schaye et al. 2014 in prep., Crain et al. 2014 in prep.). In brief, the galaxy formation physics model includes metal-dependent radiative cooling (Wiersma et al. 2009) and photo-heating in the presence of a UV and X-ray background, and the cosmic microwave background (CMB). Prior to reionization, net cooling rates are computed from the CMB and from a UV and X-ray background that follows the $z = 9$ model of Haardt & Madau (2001) with a 1 Ryd high-energy cutoff. To mimic the temperature boost due to radiative transfer and non-equilibrium effects over the optically thin limit assumed in our simulations (Abel & Haehnelt 1999), we inject 2 eV per Hydrogen and Helium atom. We assume that Hydrogen reionizes instantaneously at $z = 11.5$ (Planck Collaboration et al. 2013), while the redshift dependence of Helium reionization is modelled as a Gaussian centred at $z = 3.5$ (Theuns et al. 2002) with $\sigma(z) = 0.5$. As shown by Rollinde et al. (2013), the resultant evolution of the temperature-density relation is consistent with measurements of the intergalactic medium (Schaye et al. 2000).

Star formation follows Schaye & Dalla Vecchia (2008) with a metallicity-dependent threshold (Schaye 2004). The model includes stellar evolution (Wiersma et al. 2009) and stochastic thermal supernova feedback (Dalla Vecchia & Schaye 2012), as well as black-hole growth and AGN feedback (Rosas-Guevara et al. 2013; Booth & Schaye 2009; Springel et al. 2005).

All simulations were run twice: once with gas and the baryon physics described above, and once as dark matter only (DMO). To investigate the regime of Local Group dwarf galaxies with stellar masses below $10^8$M$_\odot$ and to demonstrate convergence, we use three different resolutions levels labelled L1, L2 and L3, whose parameters are given in Table 1. In the DMO simulations, the dark matter particle masses are larger by a factor of $(\Omega_b + \Omega_{DM})/\Omega_{DM}$ relative to the corresponding hydrodynamic simulations. For this work twelve volumes are analysed at L3, five volumes at L2, and one volume at L1. In addition, we have also rerun one volume at L3 and L2 without reionization.

We use a Friends-of-Friends algorithm (FoF, e.g. Davis et al. 1985) to identify overdense structures (FoF-groups), and the SUBFIND algorithm (Springel et al. 2001; Dolag et al. 2009) to identify self-bound substructures within them. As

**Table 1.** Numerical parameters of the simulations

| Label | Type | Particle Masses DM [M$_\odot$] | Particle Masses Gas [M$_\odot$] | Max Softening [pc] |
|---|---|---|---|---|
| L1 | hydro | $5.0 \times 10^4$ | $1.0 \times 10^4$ | 94 |
| L1 | DMO | $6.0 \times 10^4$ | – | 94 |
| L2 | hydro | $5.9 \times 10^5$ | $1.3 \times 10^5$ | 216 |
| L2 | DMO | $7.2 \times 10^5$ | – | 216 |
| L3 | hydro | $7.3 \times 10^6$ | $1.5 \times 10^6$ | 500 |
| L3 | DMO | $8.8 \times 10^6$ | – | 500 |

they represent the objects most directly associated with individual galaxies, we always refer to the self-bound substructures as "halos". For central and isolated galaxies, the terms are largely synonymous, but satellite galaxies may share the same FoF-group while still residing in separate self-bound halos.

## 3 RESULTS

### 3.1 The relevant abundance of halos

The ejection of baryons from low mass halos through heating by the UV background (Okamoto et al. 2008) and supernova feedback reduces the growth rate of a halo and, as a result, its mass in the hydrodynamic simulation is lower than that of the corresponding object in the DMO simulation. Confirming results of our previous work (Sawala et al. 2013) based on the GIMIC simulations (Crain et al. 2009), we find that the average mass of low-mass halos is reduced by up to $\sim 33\%$ relative to their counterparts in the DMO simulation. The universality of this behaviour at the low mass end, also reproduced by Munshi et al. (2013), Khandai et al. (2014), Velliscig et al. (2014), indicates that it reflects a generic effect of feedback processes and baryon physics, only weakly dependent on the particular choice and parameters of the galaxy formation model.

In the simulations with reionization, we also find that a large fraction of halos below $10^{9.5}$M$_\odot$ fail to form any stars. Photoionization has long been recognised as a possible mechanism to suppress star formation in low mass halos, through a reduction of cooling (e.g. Efstathiou 1992; Wiersma et al. 2009) and through the heating and ejection of the interstellar medium (e.g. Okamoto et al. 2008; Pawlik & Schaye 2009). It can be an important factor in establishing the number of observable dwarf galaxies in the local universe (e.g. Kauffmann et al. 1993; Bullock et al. 2000; Benson et al. 2002; Somerville 2002; Koposov et al. 2009; Okamoto & Frenk 2009).

In Fig. 1, we show the total dark matter distribution within 2 Mpc from the Local Group barycentre in one of our simulations. It can be seen that the majority of halos above $5 \times 10^7$M$_\odot$, which are highlighted in the left panel, do not contain any stars, as highlighted in the right panel. In Fig. 2 we compare the cumulative halo mass functions (left column) and halo maximum circular velocity ($v_{max}$, the circular velocity measured at the radius where $v_{circ} = \sqrt{GM(< r)/r}$ is maximal) functions (right column) obtained in the DMO and hydrodynamic simulations at $z = 0$. For the latter, we further distinguish between the total population of halos, and the population of halos that contain galaxies.
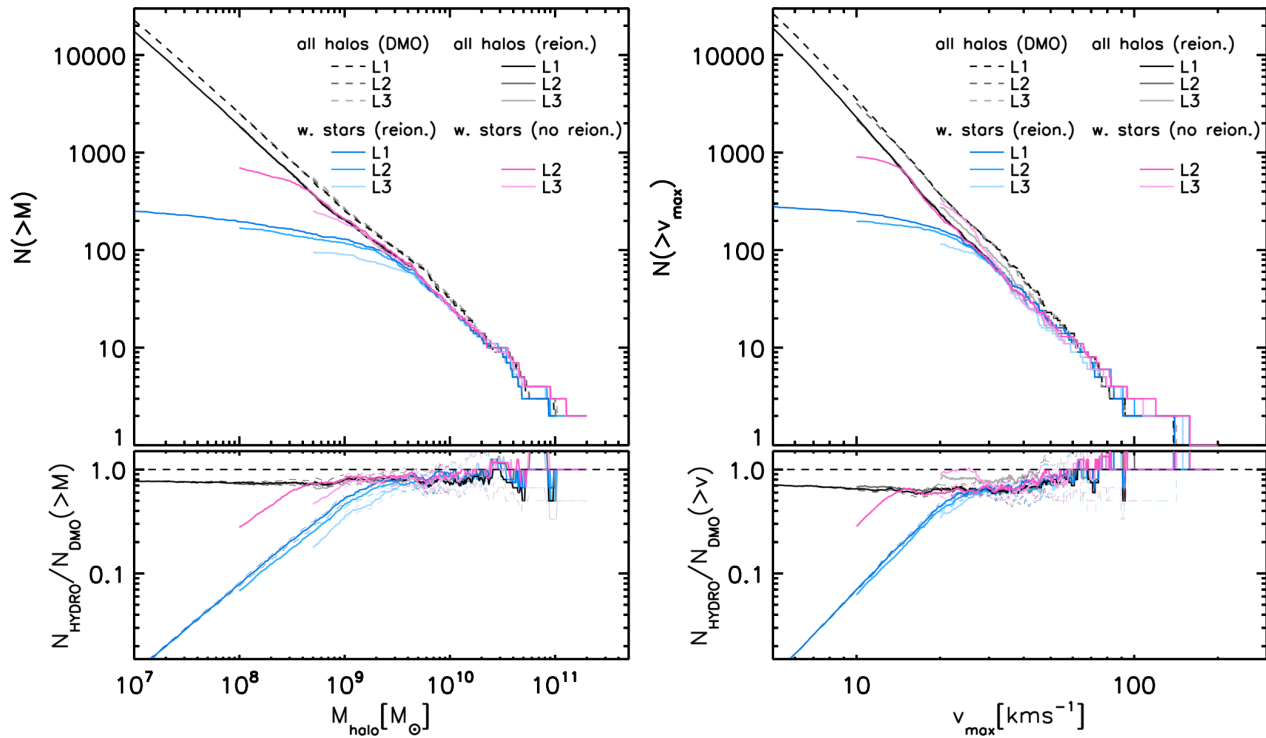
**Figure 2.** Top: cumulative halo mass function (left) and maximum circular velocity function (right) in one of our simulated LG volumes, in DMO simulations (dashed lines) and in hydrodynamic simulations (solid lines) at $z = 0$. Grey lines show the results counting all halos, while coloured lines count only halos that contain at least one star particle; blue for the simulation with reionization and purple for the simulation without reionization. In each case, lightly coloured lines are obtained from L3, medium colours from L2, and dark colours from L1. Bottom: ratio of the cumulative halo mass function (left) and maximum circular velocity function (right), relative to the DMO results. Dashed lines also indicate the $1\sigma$ scatter, from all twelve volumes at L3 for $M > 10^{10}M_\odot$, $v_{max} > 50 kms^{-1}$, five volumes at L2 for $10^9 < M < 10^{10}M_\odot$, $30 < v_{max} < 50 kms^{-1}$; and one volume at L1 for $M < 10^9 M_\odot$, $v_{max} < 20 kms^{-1}$. While the fraction of dark halos decreases significantly from L3 to L2 where the threshold stellar mass decreases from $5 \times 10^6 M_\odot$ to $4.2 \times 10^5 M_\odot$, the results are converged for L2 in the simulations that include reionization.

The bottom panels show the ratios between the cumulative mass- and velocity-functions of the hydrodynamic and DMO simulations.

In all panels different shades indicate the resolution dependence: light lines correspond to L3, intermediate to L2 and dark to L1, the highest resolution simulation. The apparent fraction of dark halos still decreases between L3 and L2, where the minimum stellar mass decreases by a factor of 12, from $\sim 1.5 \times 10^6 M_\odot$ to $\sim 1.3 \times 10^5 M_\odot$. However, a further decrease of this minimum stellar mass by the same factor to $\sim 10^4 M_\odot$ at L1 only has a very small effect on the total number of galaxies in halos above $10^8 M_\odot$, and the corresponding dark fraction. The number of "galaxies", i.e. the fraction of halos in which any stars have formed, has thus converged at L2.

In the hydrodynamic simulations, the reduced growth rate of halos below $\sim 10^{10} M_\odot$, or $v_{max}$ below $\sim 70 kms^{-1}$, results in lower masses and a reduced halo abundance. More importantly, confirming earlier results by (e.g. Crain et al. 2007; Okamoto et al. 2008; Okamoto & Frenk 2009; Pawlik & Schaye 2009), we find that reionization prevents star formation in most halos below $\sim 10^{9.5} M_\odot$ ($v_{max} \sim 25 kms^{-1}$). We find a continuous decline in the galaxy fraction, from $\sim 100\%$ of all halos at $5 \times 10^9 M_\odot$ to $< 5\%$ at $10^8 M_\odot$. Reflecting the fact that the probability of star formation strongly

depends on a halo's formation history and binding energy, the resulting decline is steeper when expressed in terms of $v_{max}$.

In the simulations without reionization, dark halos only appear for halo masses below $10^{8.5} M_\odot$ or velocities below $12 kms^{-1}$ at L2. In this (unrealistic) scenario, the total number of galaxies is not converged in our simulations, and is likely to increase further with higher resolution. By contrast, the inclusion of reionization provides an upper limit to the number of galaxies that is independent of resolution at the level reached in our simulations.

It is also worth noting that while the abundance of objects in the hydrodynamical simulations with reionization is always at or below the DMO case in terms of halo mass, it can exceed the DMO case in terms of $v_{max}$ for halos with $v_{max} >\sim 100 kms^{-1}$. In these massive halos, cooling is efficient, baryons are largely processed inside the halo, and adiabatic contraction can lead to an increase of concentration and $v_{max}$, without changing the total halo mass. We note, however, that as a result of AGN feedback, the abundance of haloes is reduced up to much higher masses (Velliscig et al. 2014; Cui et al. 2014).
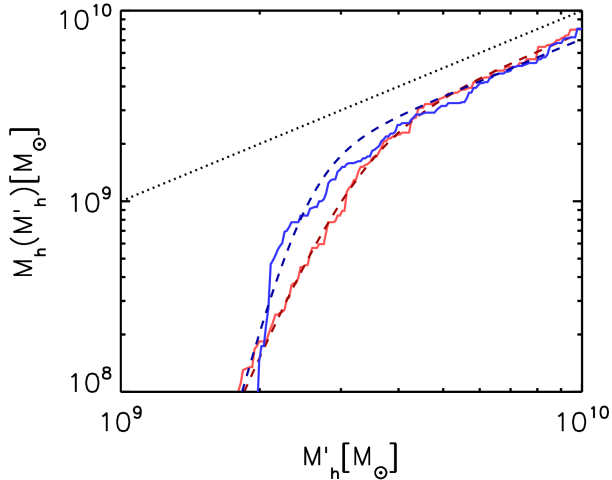
**Figure 3.** Mass of halos containing galaxies in the hydrodynamic simulation, as a function of the halo mass in the DMO simulation corresponding to the same cumulative abundance. Solid curves indicate results at $z = 0$ (red) and at peak mass (blue), dashed curves show the respective fits of Equation 3 over the plotted mass interval. For guidance, the dotted black line indicates a 1:1 relation, which corresponds to no baryon effects and all halos populated by galaxies.

## 3.2 Abundance matching in the real universe

While the reduction in average halo mass due to baryons is noticeable, the steeply declining fraction of halos that contain observable galaxies has the strongest impact on abundance matching for halos below $3 \times 10^9 \mathrm{M}_\odot$.

We stress that in order to relate observed galaxies to their dark matter halos via abundance matching, only those halos that host galaxies should be taken into account. Defining the total mass function, $N_h'(m)$, as the mass function of all dark matter halos irrespective of occupation, and the *reduced halo mass function*, $N_h(m)$, as the mass function of halos *that host galaxies*, we can derive the combined effects of the influence of baryons on halo mass, and the incomplete occupation of halos by galaxies. Matching $N_h(m)$ as measured in our hydrodynamic simulation to $N_h'(m)$ as measured in the corresponding DMO simulation,

$$\int_{\mathrm{M_h}}^{\mathrm{M_{h,max}}} N_h(m)dm = \int_{\mathrm{M_h'}}^{\mathrm{M_{h,max}'}} N_h'(m)dm, \qquad (2)$$

we can compute the mass $M_h(M_h')$ of halos containing galaxies in the hydrodynamic simulation for which the cumulative abundance equals that of all halos of mass $M_h'$ in the DMO simulation.

As shown in Fig. 3, for $M_h' = 2 \times 10^9 - 10^{10} \mathrm{M}_\odot$, we find a good fit to the relation $M_h(M_h')$ by functions of the form

$$M_h(M_h') = \frac{\alpha M_h'}{1 + (M_h'/M_0)^\beta}, \qquad (3)$$

where $0 < \alpha < 1$ and $\beta < -1$. The high mass asymptote $M_h = \alpha M_h'$ results from the reduction in halo mass by baryon effects, while the low mass asymptote $M_h = \alpha M_0^\beta M_h'^{1-\beta}$ is caused by the steep decline in the fraction of luminous halos below $M_0$. When measured at $z = 0$, we find values of $\alpha = 0.76$, $M_0 = 3.2 \times 10^9 \mathrm{M}_\odot$ and $\beta = -4.7$.

As abundance matching is commonly applied to the peak mass that a halo attains, rather than to the current mass (which can be reduced by tidal stripping after infall in the case of satellites), we repeat our analysis for the same set of halos selected at $z = 0$, but using the peak mass for both $M_h$ and $M_h'$. Here, we find values of $\alpha = 0.71$, $M_0 = 2.5 \times 10^9 \mathrm{M}_\odot$ and $\beta = -8$, but note that the luminous fraction among halos with peak masses at $\sim 10^9 \mathrm{M}_\odot$ in our simulation is so low that the value of $\beta$ is poorly constrained.

The relation $M_h(M_h')$ allows us to obtain an expression for the stellar-to-total mass relation expected in a universe with baryons and both luminous and dark halos, given a stellar-to-halo mass relation previously obtained from abundance matching, where a DMO simulation and a complete occupation of halos by galaxies had been assumed:

$$\left.\frac{m_\star}{m_H}\right|(M_h) = \left.\frac{m_\star}{m_H}\right|_{DMO}(M_h'), \qquad (4)$$

under the assumption that there is no significant change in the correlation between average halo mass and galaxy mass.

Since those halos that are predicted not to host any galaxy are excluded from the *reduced halo* mass function, galaxies are now assigned to halos of lower masses than they would have been in the DMO simulation, increasing their stellar-to-total mass ratios. By analogy, if galaxies exist that do not belong to any dark matter halos (e.g. "tidal dwarf galaxies"), we would require a *reduced galaxy* stellar mass function, with the effect of decreasing the average stellar-to-total mass ratios. However, such objects are not found in our simulations.

In Fig. 4, we show the resulting change in the stellar-to-total mass relations, with halo masses measured at peak mass (top), or at $z = 0$ (bottom). The black lines show the results based on standard abundance matching of DMO simulations by Guo et al. (2010, dashed), Wang & Jing (2010, dotted), and Moster et al. (2013, solid), while the blue line (top panel) and red line (bottom panel) show the relation of Moster et al. (2013) after our correction for baryonic effects and the presence of dark halos.

In both panels, it can be seen that the typical stellar mass of galaxies in halos of $10^9 \mathrm{M}_\odot$ is increased by an order of magnitude, and in halos of $3 \times 10^8 \mathrm{M}_\odot$, it is increased by almost two orders of magnitude. This change in the stellar-to-total mass ratio can be greater than the differences between individual abundance matching models that are shown in the top panel and which account for differences in the stellar mass function, cosmology, assumed scatter, and treatment of satellites. In other words, abundance matching applied to DMO simulations that do not account for baryons fail to constrain any of the other parameters in the dwarf galaxy regime.

It can also be seen from Fig. 4 that the faint end tail of the stellar-to-total mass relation deviates from the single power-law form which was originally introduced by Yang et al. (2003) and that is assumed in most abundance matching models.

## 3.3 Self-consistent abundance matching

The stellar and total masses measured for galaxies and halos in our simulation at L1 are indicated by circles in both pan-
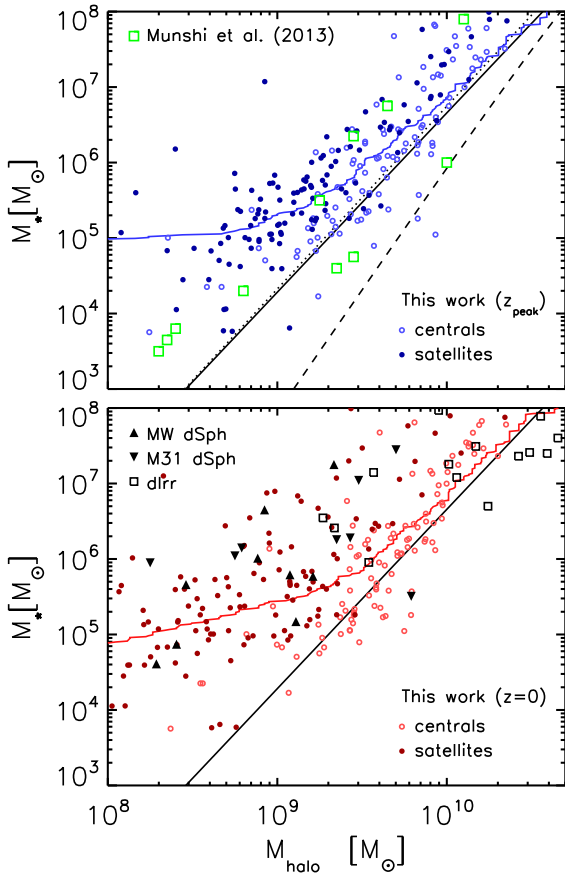
**Figure 4.** Stellar-to-total mass relation for galaxies as a function of peak halo mass (top) and of halo mass at $z = 0$ (bottom). The black lines show abundance matching results from DMO simulations by Guo et al. (2010, dashed), Wang & Jing (2010, dotted), and Moster et al. (2013, solid, reproduced in both panels). The blue solid line (top) and red solid line (bottom) show the results of Moster et al. (2013) after our correction for the effect of baryons and dark halos. In both panels, circles show the results for central galaxies (open circles) and satellite galaxies (filled circles) as measured in our simulations. In the top panel, green squares denote results of hydrodynamic simulations by Munshi et al. (2013), which are tuned to reproduce the original abundance matching relation. In the bottom panel, we compare our results at $z = 0$ to observations of individual M31 and MW dwarf spheroidal galaxies (triangles, Misgeld & Hilker (2011); Woo et al. (2008); Peñarrubia et al. (2008); Tollerud et al. (2012)), and dwarf irregular galaxies (squares, Ferrero et al. (2012); McGaugh (2005); Oh et al. (2011); Stark et al. (2009); Côté et al. (2000)).

els in Fig. 4. Both at $z = 0$ and at peak mass, these values agree well with the stellar-to-total mass relations derived from abundance matching when baryons are taken into account, as described in Section 3.2, but not with the original DMO abundance matching results.

The bottom panel of Fig. 4 also includes a comparison to observational data from Milky Way and M31 satellite galaxies, and dwarf irregular galaxies. For the MW satellites we use virial masses estimated by Peñarrubia et al. (2008), while for M31 satellites we convert $v_{max}$ estimates by Tollerud et al. (2012) using the relation for satellites given by Klypin et al. (2011). For the dwarf irregulars, we show

$m_{200}$ for the best-fitting NFW profile as measured by Ferrero et al. (2012), limiting the sample to galaxies where the velocity profile is measured to at least $r_{out} = 200pc$.

For consistency with the observations, the halo masses at $z = 0$ of individual objects in the simulation are derived using the measured maximum circular velocity converted to mass following Klypin et al. (2011). While these observed mass estimates still involve a high degree of uncertainty, our simulation and the corrected abundance matching relation are both in good agreement with the observational data. The discrepancy between abundance matching and the measurements of individual galaxies reported by Ferrero et al. (2012) is resolved once the abundance of halos is corrected.

It should perhaps also be noted that abundance matching based on DMO simulations is not entirely self-consistent: a generic prediction obtained through abundance matching is a baryon fraction of dwarf galaxies far below the universal value, which already indicates a change in total halo mass not included in the underlying DMO simulation.

Also shown by green symbols in the top panel of Fig. 4 are the results of hydrodynamical simulations by Munshi et al. (2013), which "successfully" reproduce the abundance matching relation obtained from a DMO simulation. Note here that at $2 \times 10^8 M_{\odot}$, fewer than one in ten halos host a galaxy in our simulations, whereas the relation reproduce by Munshi et al. (2013) assumes all halos to be populated. As the stellar-to-total mass ratios diverge at low masses from those obtained in our simulation (blue symbols), the assumed models of galaxy formation physics must differ. In particular, in order to satisfy the constraints imposed by abundance matching based on DMO simulations, Munshi et al. (2013) impose a very low star formation efficiency due to processes like supernova feedback. Our results suggest that a reliance on abundance matching based on DMO simulations can lead to artificial conclusions for both cosmology and astrophysics.

It is also worth noting that our simulations with reionization only predict a few hundred dwarf galaxies within a radius of 2.5Mpc of the Local Group, in contradiction with recent results obtained from DMO simulations and abundance matching by Garrison-Kimmel et al. (2014). These authors predict thousands of as-yet undiscovered faint dwarf galaxies, whereas our simulations predict that the Local Group should contain thousands of dark halos, only a small fraction of which contain galaxies.

## 4   SUMMARY

The commonly used method of abundance matching between N-body DMO simulations and the observed stellar mass function is not assumption free: it relies on the implicit assumption that structure formation can be represented by DMO simulations and that every halo hosts a galaxy. Using a set of high resolution simulations of Local Group volumes with and without baryons, we have shown that, at the low mass end, both of these assumptions are broken. Because of cosmic reionization, most halos below $3 \times 10^9 M_{\odot}$ do not contain an observable galaxy. In this regime, the median stellar-to-total mass relation inferred directly from abundance matching only applies to (mostly unobservable) halos, but has no direct application to observable galaxies.

Our simulations assume reionization in the optically thin limit without self-shielding, and radiative cooling which does not include molecular cooling at low temperatures. While these limitations may influence the impact of reionization on star formation rates in existing galaxies, the protogalaxies that are prevented from star formation in our simulations reach neither the gas densities required for self-shielding nor the metallicities required for molecular cooling after reionization. Of course, our simulations cannot resolve the formation of Pop-III stars from primordial gas. Our results also assume that reionization is uniform and local variations might change the impact for individual galaxies, but probably not enough to affect our results substantially.

By equating the cumulative abundances of objects from hydrodynamical and DMO simulations, we have shown how abundance matching results can be modified to account for baryonic effects. We stress that a reliance on the results from abundance matching obtained through dark matter only simulations can have serious consequences: it can lead to erroneous conclusions about cosmology, and, when used as a benchmark for hydrodynamic simulations or semi-analytical models, it can also lead to false conclusions about galaxy formation physics. Baryon effects have to be taken into account self-consistently for abundance matching to give a meaningful interpretation of the connection between galaxies and halos.

## ACKNOWLEDGEMENTS

## REFERENCES

Abel T., Haehnelt M. G., 1999, ApJ, 520, L13

Avila-Reese V., Colín P., González-Samaniego A., Valenzuela O., Firmani C., Velázquez H., Ceverino D., 2011, ApJ, 736, 134

Behroozi P. S., Wechsler R. H., Conroy C., 2013, ApJ, 770, 57

Benson A. J., Frenk C. S., Lacey C. G., Baugh C. M., Cole S., 2002, MNRAS, 333, 177

Booth C. M., Schaye J., 2009, MNRAS, 398, 53

Bullock J. S., Kravtsov A. V., Weinberg D. H., 2000, ApJ, 539, 517

Côté S., Carignan C., Freeman K. C., 2000, AJ, 120, 3027

Crain R. A., Eke V. R., Frenk C. S., Jenkins A., McCarthy I. G., Navarro J. F., Pearce F. R., 2007, MNRAS, 377, 41

Crain R. A., Theuns T., Dalla Vecchia C., Eke V. R., Frenk C. S., Jenkins A., Kay S. T., Peacock J. A., Pearce F. R., Schaye J., Springel V., Thomas P. A., White S. D. M., Wiersma R. P. C., 2009, MNRAS, 399, 1773

Cui W., Borgani S., Murante G., 2014, ArXiv e-prints

Dalla Vecchia C., Schaye J., 2012, MNRAS, 426, 140

Davis M., Efstathiou G., Frenk C. S., White S. D. M., 1985, ApJ, 292, 371

Dolag K., Borgani S., Murante G., Springel V., 2009, MNRAS, 399, 497

Efstathiou G., 1992, MNRAS, 256, 43P

Ferrero I., Abadi M. G., Navarro J. F., Sales L. V., Gurovich S., 2012, MNRAS, 425, 2817

Fontanot F., De Lucia G., Monaco P., Somerville R. S., Santini P., 2009, MNRAS, 397, 1776

Frenk C. S., White S. D. M., Davis M., Efstathiou G., 1988, ApJ, 327, 507

Garrison-Kimmel S., Boylan-Kolchin M., Bullock J. S., Lee K., 2014, MNRAS, 438, 2578

Guo Q., White S., Boylan-Kolchin M., De Lucia G., Kauffmann G., Lemson G., Li C., Springel V., Weinmann S., 2011, MNRAS, 413, 101

Guo Q., White S., Li C., Boylan-Kolchin M., 2010, MNRAS, 404, 1111

Haardt F., Madau P., 2001, in D. M. Neumann & J. T. V. Tran ed., Clusters of Galaxies and the High Redshift Universe Observed in X-rays Modelling the UV/X-ray cosmic background with CUBA

Hopkins P. F., 2013, MNRAS, 428, 2840

Jenkins A., 2010, MNRAS, 403, 1859

Jenkins A., 2013, MNRAS, 434, 2094

Kauffmann G., White S. D. M., Guiderdoni B., 1993, MNRAS, 264, 201

Khandai N., Di Matteo T., Croft R., Wilkins S. M., Feng Y., Tucker E., DeGraf C., Liu M.-S., 2014, ArXiv e-prints

Klypin A. A., Trujillo-Gomez S., Primack J., 2011, ApJ, 740, 102

Koposov S. E., Yoo J., Rix H.-W., Weinberg D. H., Macciò A. V., Escudé J. M., 2009, ApJ, 696, 2179

Kravtsov A. V., Berlind A. A., Wechsler R. H., Klypin A. A., Gottlöber S., Allgood B., Primack J. R., 2004, ApJ, 609, 35

McGaugh S. S., 2005, ApJ, 632, 859

Misgeld I., Hilker M., 2011, MNRAS, 414, 3699

Moster B. P., Naab T., White S. D. M., 2013, MNRAS, 428, 3121

Moster B. P., Somerville R. S., Maulbetsch C., van den Bosch F. C., Macciò A. V., Naab T., Oser L., 2010, ApJ, 710, 903

Munshi F., Governato F., Brooks A. M., Christensen C., Shen S., Loebman S., Moster B., Quinn T., Wadsley J., 2013, ApJ, 766, 56

Oh S.-H., de Blok W. J. G., Brinks E., Walter F., Kennicutt Jr. R. C., 2011, AJ, 141, 193

Okamoto T., Frenk C. S., 2009, MNRAS, 399, L174

Okamoto T., Gao L., Theuns T., 2008, MNRAS, 390, 920

Pawlik A. H., Schaye J., 2009, MNRAS, 396, L46

Peñarrubia J., McConnachie A. W., Navarro J. F., 2008, ApJ, 672, 904

Planck Collaboration Ade P. A. R., Aghanim N., Armitage-Caplan C., Arnaud M., Ashdown M., Atrio-Barandela F., Aumont J., Baccigalupi C., Banday A. J., et al. 2013, ArXiv 1303.5076

Rollinde E., Theuns T., Schaye J., Pâris I., Petitjean P., 2013, MNRAS, 428, 540

Rosas-Guevara Y. M., Bower R. G., Schaye J., Furlong M., Frenk C. S., Booth C. M., Crain R., Dalla Vecchia C., Schaller M., Theuns T., 2013, ArXiv 1312.0598

Sawala T., Frenk C. S., Crain R. A., Jenkins A., Schaye J., Theuns T., Zavala J., 2013, MNRAS, 431, 1366

Sawala T., Guo Q., Scannapieco C., Jenkins A., White S., 2011, MNRAS, 413, 659

Scannapieco C., et al., 2012, MNRAS, 423, 1726

Schaye J., 2004, ApJ, 609, 667

Schaye J., Dalla Vecchia C., 2008, MNRAS, 383, 1210

Schaye J., Dalla Vecchia C., Booth C. M., Wiersma R. P. C., Theuns T., Haas M. R., Bertone S., Duffy A. R., McCarthy I. G., van de Voort F., 2010, MNRAS, 402, 1536

Schaye J., Theuns T., Rauch M., Efstathiou G., Sargent W. L. W., 2000, MNRAS, 318, 817

Somerville R. S., 2002, ApJ, 572, L23

Springel V., 2005, MNRAS, 364, 1105

Springel V., Di Matteo T., Hernquist L., 2005, MNRAS, 361, 776

Springel V., White S. D. M., Tormen G., Kauffmann G., 2001, MNRAS, 328, 726

Stark D. V., McGaugh S. S., Swaters R. A., 2009, AJ, 138, 392

Theuns T., Schaye J., Zaroubi S., Kim T.-S., Tzanavaris P., Carswell B., 2002, ApJ, 567, L103

Tollerud E. J., Beaton R. L., Geha M. C., Bullock J. S., Guhathakurta P., Kalirai J. S., Majewski S. R., Kirby E. N., Gilbert K. M., Yniguez B., Patterson R. J., Ostheimer J. C., Cooke J., Dorman C. E., Choudhury A., Cooper M. C., 2012, ApJ, 752, 45

Vale A., Ostriker J. P., 2006, MNRAS, 371, 1173

Velliscig M., van Daalen M. P., Schaye J., McCarthy I. G., Cacciato M., Le Brun A. M. C., Dalla Vecchia C., 2014, ArXiv e-prints

Wang L., Jing Y. P., 2010, MNRAS, 402, 1796

Weinmann S. M., Pasquali A., Oppenheimer B. D., Finlator K., Mendel J. T., Crain R. A., Macciò A. V., 2012, MNRAS, 426, 2797

White S. D. M., Frenk C. S., 1991, ApJ, 379, 52

White S. D. M., Rees M. J., 1978, MNRAS, 183, 341

Wiersma R. P. C., Schaye J., Smith B. D., 2009, MNRAS, 393, 99

Wiersma R. P. C., Schaye J., Theuns T., Dalla Vecchia C., Tornatore L., 2009, MNRAS, 399, 574

Woo J., Courteau S., Dekel A., 2008, MNRAS, 390, 1453

Yang X., Mo H. J., van den Bosch F. C., 2003, MNRAS, 339, 1057